# Wrinkling evolution of a growing bubble: the wonders of petal-like patterns in amorphous silicon membranes†

**Kayoung Lee,[a] Sangwook Lee,[a] Dahl-Young Khang[b] and Taeyoon Lee*[a]**

***Received 17th February 2010, Accepted 25th March 2010***
***First published as an Advance Article on the web 17th May 2010***
**DOI: 10.1039/c003293j**

A large-area amorphous silicon (a-Si) membrane on an oxidized wafer ($SiO_2$/Si) is detached from the substrate by dissolving the sandwiched oxide layer using hydrofluoric acid solution ($HF/H_2O$). Due to the atomic disorder in the structure of a-Si, the rate of molecular diffusion inside the a-Si film and etching of the oxide layer is not uniform over the film; thus, certain over-susceptible spots for etchant infiltration starts to locally detach. Using an *in situ* optical microscope, initially the detached region is observed to be buckled as a circular dome-shaped protuberance, which then forms wrinkles around the rim of the a-Si bubble. Around the rim, the deformation pattern was strongly dependant on the thickness $h$ of the film, where the number of facets in the engendered petal-like patterns decreased with the increasing $h$. The tension-induced wrinkling in a-Si membranes was analytically and semi-quantitatively examined, and we conclude that the formation of peripheral corrugation is primarily due to the upward stretching force exerted by the underlying droplet composed of etchant and etching byproducts. The understanding of the elastic instability in ultrathin membranes could be extended to direct measurement of the fundamental properties in mechanically inferior systems.



## Introduction

Ultrathin membranes have been utilized in wide applications involving biosensors for molecular detection,[1] charge- or size-based filters,[2,3] protein transport nanochannels,[4] air-breathing fuel cells,[5,6] artificial tissues,[7] and electronic devices on a flexible substrate.[8] By the versatility of the transfer printing technique, electronics composed of heterogeneous nano-membranes in a three dimensional structure on wide classes of substrates have been especially exploited.[9] Recently, high performance silicon integrated circuits and graphene on flexible substrates has been accomplished through sacrificial layer removal and transfer printing technique.[10,11] However, the inferior mechanical properties of most ultrathin membranes require extremely careful handling, which has been the major reason as to why a technique for dealing with the membranes without applying any damages has become one of the essential issues for further mass-production of membrane-based electronics.

In transfer printing, nanomaterials are first detached from a rigid wafer. During the detachment process, becoming free and unstable, it is highly probable that the detached membrane undergoes mechanical deformations; thus, fundamental understanding of the membrane instability during the detachment process is highly necessitated. The physics on deformations including buckling and wrinkling of a thin sheet have been studied for a long time.[12] Nonetheless, it is not easy to apply the theoretical approaches to various kinds of deformations with corresponding complex geometry in the nano scale since they are described by a set of nonlinear partial differential equations, known as the Föppl–von Karman equations.[13]

In this article, we have chosen ultrathin amorphous silicon (a-Si) membranes on oxidized wafers as a model system to investigate the instability of a film during the detachment. Free a-Si membranes were obtained through etching the wafer by exposing the samples to a $HF/H_2O$ etchant that penetrates the structure of a-Si. The full courses of the a-Si film detachment was closely observed using an *in situ* optical microscope during the $HF/H_2O$ etching and our research especially focused on investigating the unique membrane deformations in the early stages of the detachment, which has still remained unexplored.

The rate of film detachment is not identical over a sample due to the variation of atomic density in an a-Si film. Thus, several over-susceptible areas for the HF permeation in an a-Si film are locally detached at first, initiating the formations of a-Si bubbles (with a domelike buckled shape) in a few μm-scale radius $L$ randomly distributed over the film. The size of an a-Si bubble increases as the etching time $t$ increases, and the aspect of the membrane deformation changes when $L \gtrsim L_c$, the critical radius of a-Si bubbles that can tolerate the formation of bubbles without any facet developments. As the process continued, symmetric facets and distinct wrinkles gradually appeared around the edge of the bubble, forming a petal-like pattern. Employing the classical theory of elastic stability[12,13] and scaling rules describing wavelength of wrinkles under tension,[13,14] the relationship between the corrugation pattern and several geometrical factors such as film thickness $h$ and the size of

[a]*Nanobio Device Laboratory, School of Electrical and Electronic Engineering, Yonsei University, 134 Shinchon-Dong, Seodaemun-Gu, Seoul, 120-749, Korea. E-mail: taeyoon.lee@yonsei.ac.kr; Fax: +82 02 313 2879; Tel: +82 2 2123 5767*
[b]*Department of Materials Science and Engineering, Yonsei University, 134 Shinchon-Dong, Seodaemun-Gu, Seoul, 120-749, Korea*
† Electronic supplementary information (ESI) available: Supplementary movies and description. See DOI: 10.1039/c003293j

a bubble were examined. For thicker membranes, the number of wrinkles $N$ decreased while the wavelength of the initial wrinkles at the rim of a bubble ($2\pi L_c/N$) increased over time.

## Experimental procedures

The sacrificial layer of 300 nm-thick silicon dioxide was grown on a silicon wafer by dry oxidation, followed by the deposition of undoped hydrogenated a-Si film through plasma enhanced chemical vapor deposition (PE-CVD) system from a gas mixture of $SiH_4$, He, and $H_2$ at 280 °C. The samples with 100, 200, 300, and 400 nm-thick a-Si films were separately prepared, and the residual stress in deposited a-Si films generated during the PE-CVD process was measured using a FLX 2320 stress measurement system (KLA Tencor) with a precision of ±5 GPa. The prepared 30 × 30 mm a-Si/$SiO_2$/Si samples were immersed in concentrated 49% hydrofluoric acid (HF) solution to dissolve the sandwiched sacrificial oxide layer and, consequently, detach the a-Si membranes.

Two separate permeation modes of etching reagent to the oxide can be expected: passing through the top a-Si layer directly or through the side edges of a sample. To exclude the infiltration of etchant into the oxide at the side edges of a sample, the edges were fully covered with silver paste so that the reagent transfer system is solely controlled by the diffusion throughout the a-Si layer.

The full phases of the film detachment were observed utilizing a digital camera mounted on an *in situ* optical microscope (Olympus BX-51). As the etching reaction was veiled with a transparent cover to protect the lens of the microscope from the attack by HF, the magnification of membrane patterns was limited by the experimental apparatus. In the course of data analysis, the size of a bubble was measured using an image processing software, Image J on Windows operating system. During the *in situ* investigation, the values of $L_c$, the critical radius at the onset of facet development at the rim of a-Si bubbles, were obtained using a reverse calculation method. Due to the little variation in the symmetry of the a-Si bubbles, the detached areas on the substrate by the formation of a-Si bubbles were manually acquired through Image J, and then the mean $L_c$ was estimated.

## Results and discussion

To better understand the mechanics during the film detachment, we observed the full courses of the film detachment. Fig. 1(a) to 1(l) are the images achieved during the detachment of 300 nm-thick a-Si films. The oxide etching reagent may locally infiltrate in advance through the regions of which atomic structure is sparse or distinctively favorable for molecules to permeate through. If the etchant first reaches into the underlying silicon dioxide at a certain site, the oxide at that specific region would be readily etched[15] and the section of the a-Si layer appears as a dark mark (indicated by an arrow in Fig. 1(b)). The size of the dark mark increases with respect to the etching time $t$, whilst the mark clearly forms a circular dome-shaped a-Si bubble, detached from a substrate by the partial removal of the oxide below the bubble.

Fig. 1(a) and 1(b) show the radial development of the wrinkles around the rim of the bubble as the bubble gradually

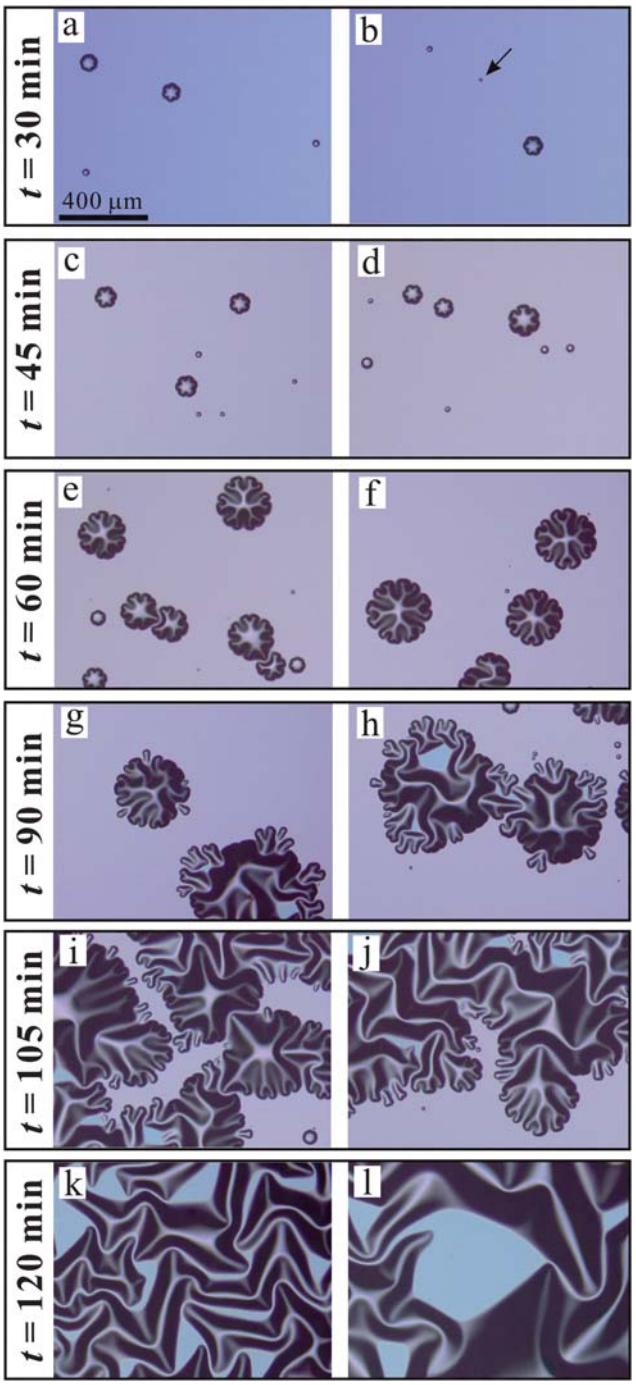


**Fig. 1** 300 nm-thick a-Si films being separated from a bulk wafer during the gradual removal of a sacrificial oxide layer. (a) and (b) images acquired at the etch time $t = 30$ min, showing the formation of bubbles. (c) and (d) images obtained at $t = 45$ min, showing that more number of bubbles appear and wrinkles of a bubble become further distinct. (e) and (f) images are obtained at $t = 60$ min, showing that the shape transition of bubbles to a dendritic form and several contiguous grown bubbles unify. (g) and (h) images are acquired at $t = 90$ min, showing that more area is detached and bubbles lose their symmetry. (i) and (j) images are acquired at $t = 105$ min, in which films are almost completely detached. (k) and (l) images are obtained at $t = 120$ min, in which film detachment is finished.

grows. The density of the bubbles increases and each wrinkle becomes further conspicuous to be a distinct branch as $t$ increases (Fig. 1(c) and 1(d)). The shape then evolves to be a dendritic one as a single branch separates into two parts and some adjacent individually detached regions are merged (Fig. 1(e) and 1(f)). Fig. 1(g) and 1(h) represent the following phase, where the a-Si film is more widely detached and the budged structure collapses, becoming no longer symmetric. The films shown in Fig. 1(i) and 1(j) are mostly detached from the mother wafers, where Fig. 1(k) and 1(l) lastly exhibit the completely detached films from the substrates, which are partially suspended. In order to obtain a robust large-area membrane, stopping the etching process at around the phase described in Fig. 1(k) to 1(l) is most preferable, since highly suspended films produced from too much dipping time are subject to tearing apart during a film transfer.

The evolved patterns similar to those of dendritic and collapsed structures in the detached a-Si membrane shown in Fig. 1(g–i) were found in other material systems and the underlying physics of their formations were extensively studied.[16–18] A. S. Argon *et al.* showed the formation of analogous blisters in as-deposited coatings of SiC on Si substrates under bi-axial compressive tension.[16] They examined the evolution of a large buckled blister in a SiC layer during the process of delamination, of which the circumferential buckling wavelength is related to the elastic properties of SiC layer and residual stress, governed by the Euler buckling relation of thin strips. Later, G. Gioia *et al.* construed the formation of buckled structures by purposely induced compressive stress on blisters of SiC diaphragms in the energy perspective: the folding patterns in SiC layers are produced to minimize the total energy of the diaphragm, which is the sum of membraneous and bending energies.[17] S. Edmonson *et al.* also reported large blisters with serious wrinkles in ultrathin polymer films (15–25 nm-thick PGMA, poly glycidyl methacrylate).[18] They showed that the structures of the created folding patterns could be determined by varying the shapes of well-defined local lateral patterns in the polymer films. Furthermore, it was explained that the development of the blister ripple is related with the stiffness and thickness of the polymer layers: the final ridge width of the blister increased linearly with respect to the film thickness $h$. However, directly applying the aforementioned mechanisms to understand the exact principles of detachment of ultrathin films using a chemical solution can be impractical. Therefore, careful observation and analysis on the full courses of the film detachment from the very initial stage is highly required.

We particularly focus on the initial formation of an a-Si bubble and the peripheral wrinkling on the bubble. A remarkable feature is revealed in Fig. 2, demonstrating a typical evolution of the wrinkles around a-Si bubbles for a range of membrane thickness from 200 to 400 nm. The shape transition of an a-Si bubble can be categorized into several steps: first, a locally detached film section forms a circular domelike shape (Fig. 2(a), 2(d), and 2(g)); next, facets slowly appear around the edge of the bubble (Fig. 2(b), 2(e), and 2(h)) as more area is detached from the substrate with increasing $t$ for $L \sim L_c$. The average values of measured $L_c$ were 32.48, 39.16, and 42.04 μm, respectively, for 200, 300, and 400 nm-thick a-Si membranes. Lastly, facets gradually become more distinct with the developing peripheral wrinkles on the bubbles and leading formation of petal-like patterns with a perfect 10, 7, and 5-fold symmetry, respectively (Fig. 2(c), 2(f), and 2(i)).

Diffusion of HF and $H_2O$ molecules occur throughout the top a-Si films with little effects on silicon,[16] when the samples are immersed in the HF solution. The etching reagent reaches the oxide layer, thereby etching the oxide according to the following reaction:[19,20]

$$\mathrm{SiO_2\ (solid) + 6HF\ (aqueous) \rightarrow H_2SiF_6\ (aqueous) + 2H_2O\ (liquid)} \quad (1)$$

$$\mathrm{SiO_2\ (solid) + 4HF\ (gas)\ or\ 2H_2F_2\ (gas) \rightarrow SiF_4\ (gas) + 2H_2O\ (gas)} \quad (2)$$

Fig. 3(a) represents the schematic illustration of the chemical reactions during the etching process of $SiO_2$ layer underneath the a-Si membrane, leading to the formation of a-Si bubbles. Owing to the local dissolution of $SiO_2$ and infiltration of HF/$H_2O$ etching reagent into the space below the detached a-Si film, a droplet ((*i*) in Fig. 3(b)) composed of water, HF, and aqueous etching byproduct $H_2SiF_6$ is yielded and trapped below the bubble. By the truncated spherical droplet kept below the a-Si bubble, oxide etching is, performed around the bottom edge of the droplet with no directional preference at the early stages, and the a-Si bubble grows maintaining the incipient circular shape.[21] As shown in Fig. 2, wrinkles gradually develop around the rim of the circular bubble as $t$ and the size of the bubble increase.

Whereas the previous models in references[16–18] suggest that the formation of buckles is solely dependent on the stress-related delamination of the membrane, we have identified two distinct elements that are responsible for the evolution of petal-like patterns in a-Si membrane. Sources of the intriguing pattern of the a-Si bubble with peripheral wrinkles can include: (1) residual compressive stress induced during the PE-CVD of the top a-Si film and (2) upward lifting and radial stretching effect in the bubble caused by the underlying $H_2O/HF/H_2SiF_6$ solution droplet inside the bubble.

During the deposition of a-Si film through PE-CVD process, a residual compressive stress σ was induced in the deposited film. This compressive stress created a uniformly distributed radial compressive force $F_r$ to be exerted from the edge to the center of a bubble as the film is detached and becomes free from a substrate. We first assume a locally detached membrane, below which the silicon dioxide layer is circularly removed, as an ideal circular plate with clamped edge and only $F_r$ is responsible for the deformations. The critical radial compressive force $F_r$, the minimum force required to buckle the film, is calculated based on the classical theory of elastic stability[12] as

$$F_{r\_cr} = \frac{14.68\ D}{L^2} \quad (3)$$

where D is the flexural rigidity (also called as the bending stiffness) of a film described as $D = Eh^3/12(1 - \nu^2)$ (E is Young's modulus and $\nu$ is Poisson ratio). Given $F_r = \sigma \cdot 2\pi L \cdot h$ and using literature values of $E \approx 80 \pm 20$ GPa and $\nu \approx 0.22$,[22] the membrane is buckled when $L$ reaches $L_{c\_buckling}$, the critical radius for the membrane to be firstly buckled as a domelike shape

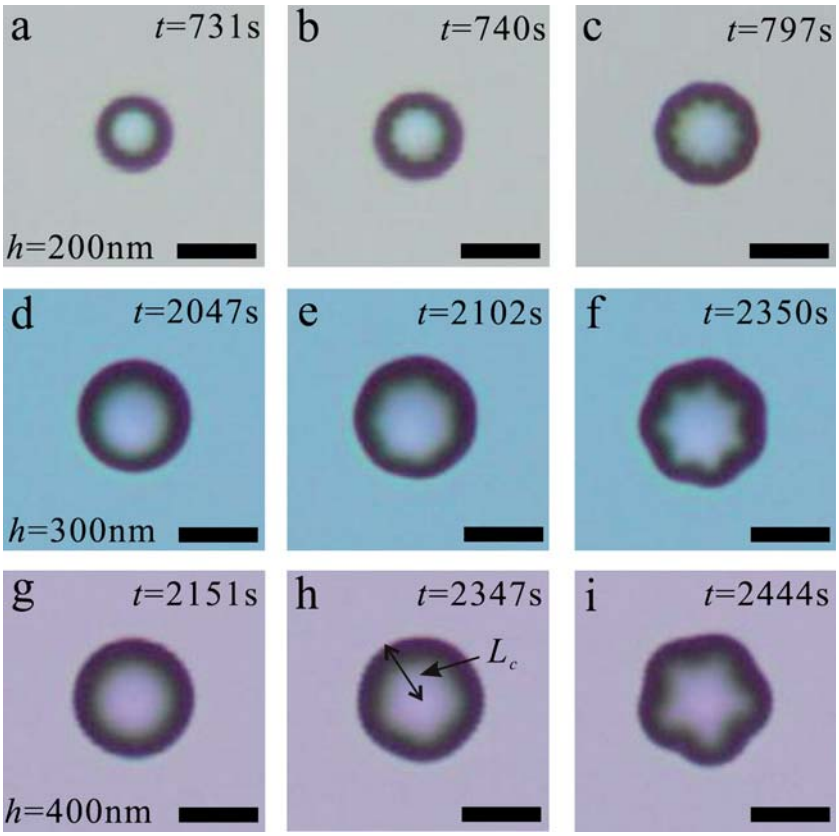


**Fig. 2** Images showing the evolution of peripheral wrinkles around the rim of bubbles as $t$ increases. The thickness of films $h$ is 200, 300, and 400 nm, respectively, for (a)–(c), (d)–(f), and (g)–(i). Initially, the locally detached films form a shape of circular domelike pattern ((a), (d), and (g)). As $t$ increases with $L \gtrsim L_c$, facets slowly appeared ((b), (e), and (h)) and, then, the wrinkles around the rim of bubbles become distinct ((c), (f), and (i)). The scale bars in images indicate 50 μm.

$$L_{c\_buckling} = 1.327^3\sqrt{\frac{D}{\sigma h}} = 1.327^3\sqrt{\frac{Eh^2}{12(1-\nu^2)\sigma}}$$

$$= 2.539 \times 10^3\left(\frac{h^2}{\sigma}\right)^{\frac{1}{3}}$$

When $L \gtrsim L_{c\_buckling}$, membranes cannot tolerate the compressive force any more, and the stress is released by generating out-of-plane displacement. Since σ was measured as approximately $-330 \pm 5$, $-310 \pm 5$, and $-300 \pm 5$ GPa, respectively for 200, 300, and 400 nm-thick films, the estimated values of $L_{c\_buckling}$ for the films of corresponding thickness are 12.57, 16.81, and 20.59 μm individually. However, bubbles with a radius below 5 μm were easily observed in the entire *in situ* experiments, and it was not observed that the size was dependent on the film's thickness. The discrepancy between the estimated $L_{c\_buckling}$ and measured value means that the residual radial compressive stress on a bubble does not mainly dominate the bubble formation, and additional sources should be considered as contributing factors to the membrane deformation.

Being detached from a substrate, an a-Si membrane can be somewhat expanded as the residual stress is released. Volker Ziebart *et al.*[23] investigated the buckling of an expanded square SiN membrane, which was compressively prestressed during the PE-CVD process of the SiN. Since the distance from the center to corner of a square membrane is longer than that from the center to other edges, buckles were strongly generated near each corner by larger strain dissipation than other regions. On the other hand, our a-Si film is detached circularly and, thus, the corresponding expansion of a circular membrane cannot be related with the radially developed deformation near the edges of an a-Si bubble. Hence, the intriguing membrane deformation shown on the rim of a bubble can be understood as not to be buckling, by compression, but to be wrinkling, by stretching.[14]

The model to explain the wrinkling evolution at the rim of an a-Si bubble is illustrated in Fig. 3(b). As described in the schematic, an a-Si bubble is propped up by an underlying $H_2O$/HF/$H_2SiF_6$ solution droplet and forms a circular dome shape. The solution drop inside this bubble has a little wetting due to the hydrophobic nature with a-Si membrane and Si substrate, causing the drop to ball up highly and stretch the a-Si bubble upward tightly. The quantity of liquid influx by HF and water molecules into the a-Si bubble is larger than that of the outflux and, therefore, the droplet and the bubble initially grows gradually. The net flux of etching agent determines the size of the underlying drop and the angle $\theta$, by which the detached a-Si membrane is deflected from the original flat position as indicated in Fig. 3. The rate of liquid flux, both the inward and outward direction, has an inverse relationship to $h$. The difference between the liquid influx and outflux is greater for thinner membranes, meaning that more liquid droplets remain below the



 

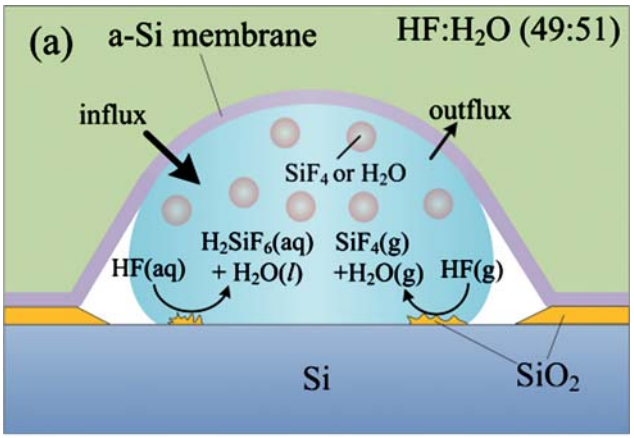


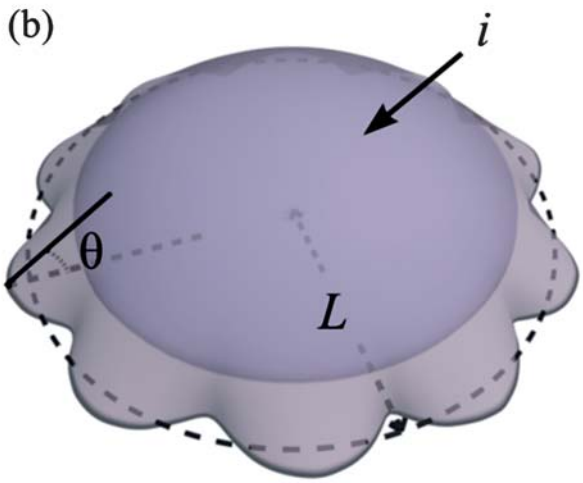


**Fig. 3** (a) Schematic representation of the chemical reaction during the initial stages of wet etching process of $SiO_2$ layer by HF. (b) Illustration depicts the formation of a bubble with 10 wrinkles. (*i*) indicates an underlying $H_2O/HF/H_2SiF_6$ solution droplet inside an a-Si bubble. By hydrophobic surface of the a-Si bubble, the drop balls up highly and propped up the bubble. $L$ and $\theta$ are also described in the figure.

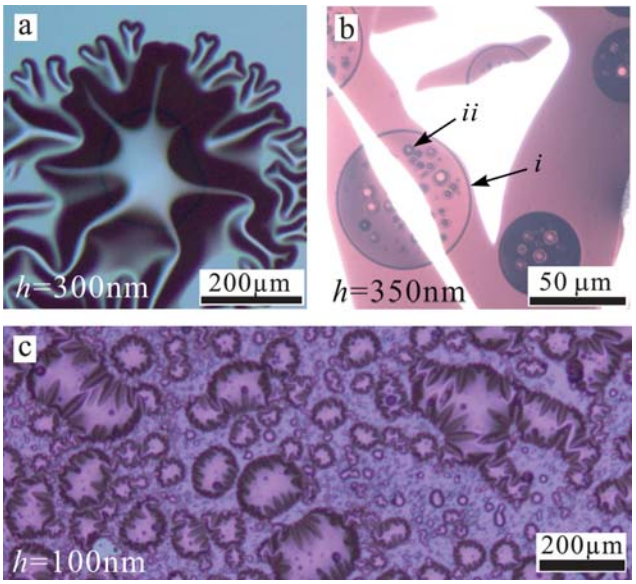


**Fig. 4** (a) A $H_2O/HF/H_2SiF_6$ solution droplet is trapped below the locally detached film and induces the bubble to have a circular shape. The image is obtained when a bubble is highly grown that an underlying droplet is vivid. A black curved line inside a bulged film designates the liquid drop. The thickness of the film is 300 nm. (b) Several liquid droplets lie down between an almost fully detached a-Si film and a substrate. (*i*) indicates an underlying liquid drop below the film and (*ii*) is gaseous byproduct captured inside the droplet. The thickness of the film is 350 μm. (c) Upwardly swelled 100 nm-thick a-Si film by gaseous byproduct from etching reagent. The degree of swelling by generated vapor pressure is the most distinct by the lowest thickness of the film in this work. The density of bubbles is so high that most bubbles merge rapidly and lose their initial circular shape.

thinner membranes. A smaller amount of liquid droplet exists below the thicker membranes, which is the reason why the induced bubbles show smaller $\theta$ and lower uplifting for the case of thicker membranes as compared to thinner membranes. Fig. 4(a) shows a trapped droplet inside an a-Si bubble clearly. The shape of the droplet is observed as a black closed curved line inside the a-Si bubble. The detached a-Si film in Fig. 4(a) is partially collapsed because the droplet cannot support the film any more and the collapsed part, the rim of the a-Si bubble, forms buckles. Fig. 4(b) represents several droplets observed when an a-Si film is fully detached.

In addition to the solution droplet, vapor pressure, induced by HF and gaseous byproduct $SiF_4$ of the etching reaction, also stretches the detached light membrane upward.[24] Fig. 4(c) presents 100 nm-thick a-Si bubbles highly swelled by volatile gas production. The resistance to the upward stretching is small owing to the low thickness of the film and, hence, $\theta$ enlarges from the vapor pressure blowing up the bubbles highly. Since most bubbles merge and then lose the incipient circular shape in a short initial transient due to the excessive density of bubbles in the case of 100 nm-thick membranes, we exclude the quantitative analysis on the 100 nm-thick bubbles. Some amount of gaseous byproduct is trapped inside a $H_2O/HF/H_2SiF_6$ solution droplet as shown in Fig. 4(b)-ii.

Fig. 5 reveals a strong evidence leading to the fact that the formation of wrinkles can be primarily attributed to the uplifting force exerted on the a-Si film from the trapped byproducts underneath the a-Si membrane. It represents 100 nm-thick a-Si bubbles that were under ambient conditions during 24 h, from which a solution drop and gases inside the bubbles had diffused out. Whereas all the other bubbles presented in this article were formed by soaking the samples in $HF/H_2O$ solution, only bubbles on Fig. 5 were originally obtained by exposing samples under gaseous $HF/H_2O$ conditions for approximately 20 s. The bubbles collapsed as the substances inside the bubbles leaked out at air conditions. Hence, the subsidence of the a-Si bubbles indicates that the formation of the bubble is dominated by the gaseous and liquid propping substances trapped in the bubbles, rather than the residual compressive stress. Prior to being exposed to the ambient conditions, all the bubbles in Fig. 5(a) to 5(c) had no wrinkles. However, bubbles large enough (Fig. 5(b) and 5(c)) generated several symmetrically arranged petals around the rim of the bubbles during their subsidence. We consider that bubbles were somewhat grown even at ambient air by the etching reagent leftover inside the bubbles until the extinction of HF, leading to the development of wrinkles. The smallest bubble

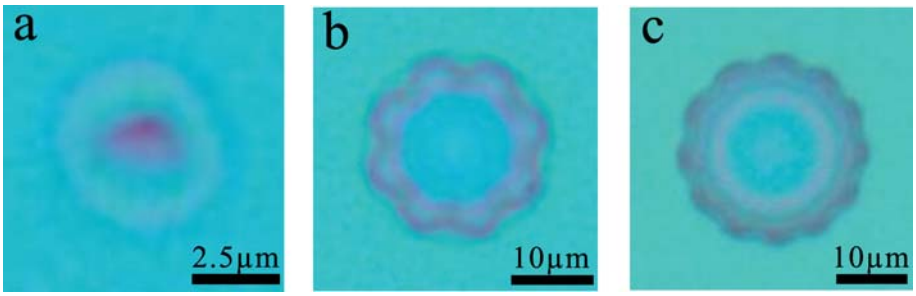


**Fig. 5** Collapsed 100 nm-thick a-Si bubbles after being under ambient conditions during 24 h. The small a-Si bubble shown in (a) collapsed maintaining its original circular shape. On the other hand, the larger bubbles in (b) and (c) evolve to a petal-like formation during their subsidence. Larger bubbles generate more number of petals, and 8 and 12 petals are formed, respectively, for the bubbles in (b) and (c).



shown in Fig. 5(a) collapsed retaining its beginning circular shape; but, larger bubbles in Fig. 5(b) and 5(c) evolved, respectively, 8 and 12 petals. As the size of the bubble increased, the number of petals also increased.

While an a-Si bubble is exposed to $HF/H_2O$, the $H_2O/HF/H_2SiF_6$ solution droplet inside the bubble and the corresponding a-Si bubble progressively grow in size. Owing to the increasing underlying droplet and vapor pressure, the bubble is gradually uplifted and consequent $\theta$ is also slowly enlarged. By the uplifting, the bubble is radially stretched with a radial stretching strain $\gamma$ and a radial stress $\sigma_r$ exerted radially on the bubble. To alleviate the increasing strain, wrinkling is gradually engendered radially around the near edge of the bubble with wavelength $\lambda$ as the bubble grows with respect to $t$, and such relationship can be explicitly explained through the equation as follows:[14]

$$\lambda \sim \left(\frac{D}{\sigma_r}\right)^{1/4} r^{1/2}, \tag{5}$$

where $r$ is the radial coordinate from the center of a bubble. We approximate the shape of a bubble to be a shallow circular cone, which has a bottom radius $L$ and a height $L\cdot\tan\theta$. From this approximation, resulting $\sigma_r$ can be described as

$$\sigma_r \sim E\gamma/L^2, (L > 0) \tag{6}$$

where a radial stretching strain $\gamma$ is denoted as

$$\gamma = \frac{1-\cos\theta}{\cos\theta}. \tag{7}$$

Here, the stretching strain can be expressed as the ratio of total deformation to the initial dimension of the material body subject to the applied force. Hence, that radial stretching strain $\gamma$ can be simplified as

$$\gamma = \frac{\delta L}{L_b} = \frac{L_a - L_a\cos\theta}{L_a\cos\theta} = \frac{1-\cos\theta}{\cos\theta},$$

where $L_b$ is the radius of the bubble before being stretched and $L_a$ is the radius of the streched bubble. In the early growth phase (before the wrinkles are developed), $\theta$ and corresponding $\gamma$ are progressively increased. When such a membrane is subject to a stretching strain, it stays tightly stretched for $\gamma < \gamma_c$, a critical stretching strain. Further stretching triggers the membrane to wrinkle.[14] Using the proposed geometric simplification, we formulate $\lambda$ to be

$$\lambda \sim \frac{rh^{3/4}}{((1-\nu^2)\gamma)^{1/4}} = \frac{rh^{3/4}}{((1-\nu^2)(1-\cos\theta)/\cos\theta)^{1/4}} \tag{8}$$

and, as $\lambda = 2\pi r/N$, corresponding $N$

$$N = \frac{2\pi r}{\lambda} \sim \frac{((1-\nu^2)\gamma)^{1/4}}{h^{3/4}} = \frac{((1-\nu^2)(1-\cos\theta)/\cos\theta)^{1/4}}{h^{3/4}} \tag{9}$$

Since stretching force is much more distributed in a transversal direction to $r$ as $L$ increases, radial stress decreases (eqn (6)) and wavelength increases as more distant from the center of a bubble (eqn (5) and eqn (8)) at a small range of $\theta$. Since a thicker bubble has lower $\theta$ and, consequently, lower $\gamma$ (by larger stretching resistance and larger liquid outflux from the bubble), the number of wrinkles $N$ in eqn (9) decreases with increasing $h$.

Fig. 6(a) exhibits the experimental results of $N$ and $\lambda$ at $r \sim L$ for the growing bubbles as a function of $Lh^{3/4}((1-\cos\theta)/\cos\theta)^{-1/4}$. The obtained data for different bubbles with different $h$ and $N$ collapses onto a single line (the dashed line on Fig. 6(a)), which confirms the theoretically estimated scaling in eqn (8) $\lambda \sim Lh^{3/4}((1-\cos\theta)/\cos\theta)^{-1/4}$ and supports the above simplified tension-governing model. A similar modeling on the relationship between the thickness of the film and generated wavelength of the delaminated structure was suggested in previous research of liquid blister test by J. Chopin *et al.*[25] Specifically, they investigated the instability of blisters on a thin elastic sheet adhering to a stiff substrate generated by imposing a vertical displacement at the center of the sheet in macroscopic scale. Interestingly, it can be seen that despite the different inherent material properties and binding forces between the substrate and thin films used in the liquid blister test and our experiments, similar relationships exist between the wavelength of the engendered deformations and the exerted uplifting force. For a comparative analysis, the appropriate data set are retrieved from the work of J. Chopin *et al.* and re-calculated by eqn (8). The results using the data sets of low density polyethylene film (LDPE) and polypropylene film (PP) are plotted on the top right corner of Fig. 6(a): as the values of $Lh^{3/4}((1-\cos\theta)/\cos\theta)^{-1/4}$ increased from 70 to 80 μm, the estimated values of wavelength for a 30 μm-thick LDPE film increased from 5.568 to 10.709 mm; for a 40 μm-thick PP film, the values increased from 12.899 to 15.475 mm. It can be seen that the slopes of the fitted lines are lower for LDPE and PP films as compared to that of the a-Si films. It can be intuitively predicted that the difference in their bending modulus D in eqn (5),

 

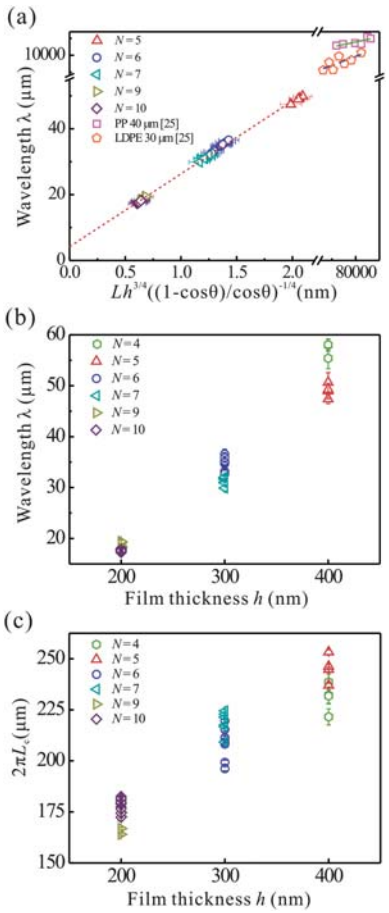


**Fig. 6** (a) Wavelength $\lambda$ and the number of wrinkles $N$ at the near edge of a bubble as a function of $Lh^{3/4}((1 - \cos\theta)/\cos\theta)^{-1/4}$. Note that $\lambda \sim Lh^{3/4}((1 - \cos\theta)/\cos\theta)^{-1/4}$ in accordance with eqn (8) which is obtained from our simplified model with geometrical approximation and exclusion of other factors save for radially induced tension $T$ on a bubble. The dashed line fitted using least-squares analyses $\lambda = 2.2 \times 10^4\ Lh^{3/4}((1 - \cos\theta)/\cos\theta)^{-1/4}$. The scattered points with linear approximation on the top right corner represent the data set taken from ref. 25 and re-calculated using eqn (8) to comparatively analyze the properties of other films in the macro scale. The open squares and circles represent the results for 30 μm-thick LDPE and 40 μm-thick PP films, respectively. The dash-dotted and solid lines fitted using least-squares analyze $\lambda_b = 66\ Lh^{3/4}((1 - \cos\theta)/\cos\theta)^{-1/4}$ and $\lambda_g = 36\ Lh^{3/4}((1 - \cos\theta)/\cos\theta)^{-1/4}$, respectively. (b) $\lambda$ at $r \approx L \approx L_c$ as a function of $h$. (c) $2\pi L_c$ with respect to $h$.

which includes the elastic modulus and poisson's ratio, played a substantial role in determining the rate of wrinkle development and the consequent values of the wavelengths. In addition, the interfacial bonding strength in our a-Si/$SiO_2$/Si system and in Chopin's system of different polymer films/adhesion layer/substrate is dissimilar. In the liquid blister test the interfacial layer between the polymer films and the substrate is composed of liquid ethanol, which adds a sliding nature of the polymer films, but a-Si membranes are firmly bonded to the Si substrate *via* $SiO_2$-based interfacial layer. Hence, the resistive force against mechanic deformation is much greater in our sample of tightly bonded a-Si/$SiO_2$/Si interface. Nonetheless, the similarity in the linear tendency proposes that our suggested model can be expanded from ultrathin nano-scale a-Si membranes to macro-scale polymer layers, meaning that it can be applicable to describe the complex mechanical fundamentals during membraneous deformations of other materials.

Fig. 6(b) shows the experimental data of $N$ and $\lambda$ at $r \sim L_c$ as a function of $h$. The membranes for different $h$ generate bubbles with different $N$: 200 nm-thick membranes produced 9 or 10 wrinkles, 300 nm-thick membranes produced 6 or 7 wrinkles, and 400 nm-thick membranes produced 4 or 5 wrinkles. The variation of $N$ within the same $h$ can be primarily attributed to a little deviation of atomic density in the a-Si membranes, which can affect the membrane properties including E and $\nu$. However, all the cases generally satisfy the linear relationship between $\lambda$ and $Lh^{3/4}((1 - \cos\theta)/\cos\theta)^{-1/4}$. Fig. 6(c) represents $2\pi L_c$ as a function of $h$. As a bubble increases (as $L$ increases), both $\theta$ and $\gamma$ gradually increase in the early stage. When $L \sim L_c$, $\theta$ reaches $\theta_c$, the critical value of $\theta$ in the present study, and the consequent $\gamma$ also reaches $\gamma_c$; then, wrinkles are engendered in a bubble to accommodate $\gamma_c$. The correspondence of $L_c$ with $h$ is governed by the kinetics in diffusion process of etchant through the membrane. The quantity of liquid droplets entrapped inside an a-Si bubble is larger in thinner membranes compared to thicker membranes. The higher influx rate, hence the higher growth rate of the bubble in thinner membranes contributes to fast reaching of $L_c$, $\theta_c$, and in turn, $\gamma_c$. On the contrary, the lower growth rate in thicker membranes allows bubbles to obtain larger $L_c$. Thus, as depicted in Fig. 6(c), the onset of bubble radius to start wrinkling $L_c$ increases with $h$.

For the analysis of these results in energy perspective, we follow E. Cerda *et al.*[26] in modeling the mechanical deformations during the initial evolution stages of a-Si films. For $L < L_c$ (in other words $\gamma < \gamma_c$), the rim of an a-Si bubble tolerates the radial strain $\gamma$ and stays tightly stretched. However, as $L$ approaches $L_c$, the enlarged uplifting force causes $\theta$ and consequent $\gamma$ to increases, and the formation of wrinkles starts as to alleviate the radial strain $\gamma$. The wavelength of the developed wrinkles is determined from a minimization of the stretching along their length and bending transverse to the wrinkles. The total elastic energy can be described as $U_{tot} = U_b + U_s$,[26] where $U_b$ is elastic potential energy due to bending transverse to the tension-field (out-of-plane deformation transverse to the folds) and $U_s$ is elastic potential energy due to stretching along the tension-field (in-plane deformation along the folds). A radially developed strain on an a-Si bubble contributes to $U_s$ in the membrane, and it can be alleviated by triggering the wrinkles when $\gamma \sim \gamma_c$.[14] In a shorter wavelength, $U_b$ is augmented further, while strain and $U_s$ is released further since the amplitude of the wrinkles decreases as the wavelength decreases. The wavelength of the wrinkles is balanced in the way of attaining the minimization of $U_{tot} = U_b + U_s$. $U_b$ is far more sensitive to the thickness of a membrane than $U_s$;[23] thus, if the wavelength of the wrinkles in the thicker a-Si bubbles decreases greatly, $U_b$ and eventually $U_{tot}$ increase greatly due to their higher bending stiffness. Accordingly, the thicker a-Si bubble generates wrinkles with longer wavelengths than the thinner one as exhibited in Fig. 2 and Fig. 6(b).

## Conclusions

We performed the detachment of a large-area a-Si membrane through the removal of the sacrificial oxide layer below the objective film and precisely observed the striking tension-field

phenomenon occurred in the detachment. The peripheral corrugation in a circular a-Si membrane with a specific three-dimensional microstructure growing in size with $t$ (we called this structure as an a-Si bubble) was both quantitatively and qualitatively analyzed. The a-Si bubble first grows in a perfect circular domelike shape by an etchant drop trapped inside the a-Si bubble and the underlying $H_2O/HF/H_2SiF_6$ solution droplet inside the bubble primarily stretched the bubble upward. Then, wrinkles are gradually engendered peripherally on the bubble for the minimization of total elastic energy. As $t$ increases further, a-Si bubbles with petal-like wrinkles progressively grow and/or they merge with other bubbles, evolving to the buckled and collapsed structures. The corrugation effect on amorphous silicon membranes by tension-field during the detachment was examined based on the physics of elastic stability. The present work provides a fundamental insight of the elastic instability of a-Si membranes, which enables us to obtain large-area intact ultra-thin membranes in mechanically inferior systems through a transfer printing technique.



## Acknowledgements

This research was supported by System IC 2010 program of the Ministry of knowledge economy, Republic of Korea [10030517-2008-02, Advanced CMOS image sensor using 3D integration], and by Priority Research Centers Program through the National Research Foundation of Korea (NRF) funded by the Ministry of Education, Science and Technology [2009-0093823].

## References

1 Guoguang Rong, Judson D. Ryckman, Raymond L. Mernaugh and Sharon M. Weiss, *Appl. Phys. Lett.*, 2008, **93**, 161109.
2 Christopher C. Striemer, Thomas R. Gaborski, James L. McGrath and Philippe M. Fauchet, *Nature*, 2007, **445**, 749.
3 Albert van den Berg and Matthias Wessling, *Nature*, 2007, **445**, 726.
4 Francesco Amato, Carlo Cosentino, Sabrina Pricl, Marco Ferrone, Maurizio Fermeglia, Mark Ming-Cheng Cheng, Robert Walczak and Mauro Ferrari, *Biomed. Microdevices*, 2006, **8**, 291.
5 V. A. Lifton, J. A. Taylor, B. Vyas, P. Kolodner, R. Cirelli, N. Basavanhally, A. Papazian, R. Frahm, S. Simon and T. Krupenkin, *Appl. Phys. Lett.*, 2008, **93**, 043112.
6 Hexiang Zhong, Xiaobo Chen, Huamin Zhang, Meiri Wang and Samuel S. Mao, *Appl. Phys. Lett.*, 2007, **91**, 163103.
7 Kirill Efimenko, Mindaugas Rackaitis, Evangelos Manias, Ashkan Vaziri, L. Mahadevan and Jan Genzer, *Nat. Mater.*, 2005, **4**, 293.
8 Yugang Sun and John A. Rogers, *Adv. Mater.*, 2007, **19**, 1897.
9 Jong-Hyun Ahn, Hoon-Sik Kim, Keon Jae Lee, Seokwoo Jeon, Seong Jun Kang, Yugang Sun, Ralph G. Nuzzo and John A. Rogers, *Science*, 2006, **314**, 1754.
10 Dae-Hyeong Kim, Jong-Hyun Ahn, Won Mook Choi, Hoon-Sik Kim, Tae-Ho Kim, Jizhou Song, Yonggang Y. Huang, Zhuangjian Liu, Chun Lu and John A. Rogers, *Science*, 2008, **320**, 507.
11 Keun Soo Kim, Yue Zhao, Houk Jang, Sang Yoon Lee, Jong Min Kim, Kwang S. Kim, Jong-Hyun Ahn, Philip Kim, Jae-Young Choi and Byung Hee Hong, *Nature*, 2009, **457**, 706.
12 Stephen P. Timoshenko, and James M. Gere, *Theory of Elastic Stability*, p. 389, McGraw-Hill Kogakusha, Ltd., New York, 1961.
13 E. Cerda and L. Mahadevan, *Phys. Rev. Lett.*, 2003, **90**, 074302.
14 Jiangshui Huang, Megan Juszkiewicz, Wim H. de Jeu, Enrique Cerda, Todd Emrick, Narayanan Menon and Thomas P. Russell, *Science*, 2007, **317**, 650.
15 Kirt R. Williams, Kishan Gupta and Matthew Wasilik, *J. Microelectromech. Syst.*, 2003, **12**(6), 761.
16 A. S. Argon, V. Gupta, H. S. Landis and J. A Cornie, *J. Mater. Sci.*, 1989, **24**, 1207.
17 G. Gioia, A. DeSimone, M. Ortiz and A. M. Cuitiño, *Proc. R. Soc. London, Ser. A*, 2002, **458**, 1223.
18 S. Edmondson, K. Frieda, J. E. Comrie, P. R. Onck and W. T. S. Huck, *Adv. Mater.*, 2006, **18**, 724.
19 James W. Mayer and S. S. Lau, *Electronic Materials Science: For Integrated Circuits in Si and GaAs*, Macmillan, 1990, New York.
20 R. Hull, *Properties of Crystalline Silicon*, 4th edn, IET, 1999.
21 Because etch rate of thermal oxide by concentrated 49% HF is 2300 nm $min^{-1}$ [Kirt R. Williams, Kishan Gupta and Matthew Wasilik, *J. Microelectromech. Syst.*, 2003, **12**(6), 761] and that of covered oxide by another layer further increases [E. Stolyarova, D. Stolyarov, K. Bolotin, S. Ryu, L. Liu, K. T. Rim, M. Klima, M. Hybertsen, I. Pogorelsky, I. Pavlishin, K. Kusche, J. Hone, P. Kim, H. L. Stormer, O. V. Yakimenko and G. Flynn, *Nano Lett.*, 2009, **9**(1), 332–337], atomic density (or homogeneity) of sandwitched $SiO_2$ does not much affect the shape of a bubble.
22 L. B. Freund and S. Suresh, *Thin film materials*, p. 96, Cambridge University Press, Cambridge, 2003.
23 Volker Ziebart, Oliver Paul and Henry Baltes, *J. Microelectromech. Syst.*, 1999, **8**(4), 423.
24 E. Stolyarova, D. Stolyarov, K. Bolotin, S. Ryu, L. Liu, K. T. Rim, M. Klima, M. Hybertsen, I. Pogorelsky, I. Pavlishin, K. Kusche, J. Hone, P. Kim, H. L. Stormer, O. V. Yakimenko and G. Flynn, *Nano Lett.*, 2009, **9**(1), 332.
25 J. Chopin, Dominic Vella and Arezki Boudaoud, *Proc. R. Soc. London, Ser. A*, 2008, **464**, 2887.
26 E. Cerda, K. Ravi-Chandar and L. Mahadevan, *Nature*, 2002, **419**, 579.

 